Temperature dependence and capping and underlayer layers effect on the interfacial magnetic properties of Ir/Fe-or Pt/Fe-based systems

Djoudi Ourdani, N Challab, Yves Roussigné, Salim Mourad Chérif, Mihai Sebastian Gabor, Mohamed Belmeguenai

Temperature dependence and capping and underlayer layers effect on the interfacial magnetic properties of Ir/Fe- or Pt/Fe-based systems

Djoudi Ourdani[1], N. Challab[1], Yves Roussigné[1], Salim Mourad Chérif[1], Mihai Sebastian Gabor[2,*]and Mohamed Belmeguenai [1,**]

[1] Université Sorbonne Paris Nord, *LSPM, CNRS, UPR 3407, F-93430 Villetaneuse, France*

[2] *Center for Superconductivity, Spintronics and Surface Science, Physics and Chemistry Departament, Technical University of Cluj-Napoca, Str. Memorandumului No. 28 RO-400114 Cluj-Napoca, ROMANIA*

Abstract- Brillouin light scattering and microstrip line ferromagnetic resonance were used to investigate the perpendicular magnetic anisotropy (PMA), the magnetic damping and the interfacial Dzyaloshinskii-Moriya interaction (iDMI) in X/Fe(t_{Fe})/Y thin films of variable thickness (1.4 nm≤t_{Fe}≤10 nm), where X=Pt, Ir or Cu and Y=Ir, Cu or MgO. A particular interest is given to their temperature dependence. A method was devised to accurately determine the individual contribution of each interface with Fe to the effective interface PMA constant. This involved combination of the direct measurement of the thickness dependences of effective magnetization and frequency mismatch. We observed an asymmetrical Ir/Fe and Fe/Ir as well as Cu/Fe and Fe/Cu interfaces: Fe/Ir contributes strongly in PMA and spin pumping induced damping. The damping constant dependence on the inverse effective thickness of Fe revealed a nonlinear behavior, attributed to the interfacial two magnon scattering, found to be strong in Cu/Fe/Ir and Cu/Fe/Cu. iDMI measurements revealed an opposite chirality of Pt/Fe and Ir/Fe interfaces. These magnetic interfacial properties were studied as a function of temperature in the Pt/Fe/Cu and Cu/Fe/Cu systems. We showed that the interface PMA constant increases linearly with temperature, while iDMI constant decreases significantly, in absolute value, by approximately 60%. This behaviou is most probably due to thermal disorder, suggesting a greater sensitivity of iDMI to temperature. Measurements post-temperature indicated that the temperature triggers interdiffusion and affects the magnetic properties. However, it is difficult to dissociate them due to the absence of in-situ VSM measurements.

Keywords: Damping, Perpendicular magnetic anisotropy, spin pumping, Ferromagnetic resonance, Brillouin light scattering, Interfacial Dzyaloshinskii-Moriya interaction.
* mihai.gabor@phys.utcluj.ro, ** belmeguenai.mohamed@univ-paris13.fr

I- Introduction

The spin-orbit interaction, which couples the orbital motion of electrons to their spins, is associated with several crucial phenomena in magnetism. Consequently, it offers a promising avenue for the creation of innovative spintronic devices [1]. Recent discoveries highlight that the interface between ferromagnetic metal (FM) and heavy metal (HM) hosts a diverse range of significant phenomena linked to spin-orbit coupling. These include spin-orbit torque [2], interfacial perpendicular magnetic anisotropy (PMA) [3-5], spin-pumping-induced damping [6], interfacial Dzyaloshinskii-Moriya interaction (iDMI) [7], and spin-current generation [8]. These phenomena are expected to play a crucial role in advancing the next generation of spintronic devices, characterized by improved performance (faster and denser) with a reduced power consumption, ultimately determining the feasibility and the success of these technologies.

iDMI is a relatively recent emerging phenomenon that significantly influences the static and dynamic magnetic characteristics of FM/HM ultrathin film systems. It modifies the static and dynamic behaviors of domain walls [9], induces non-reciprocal spin wave propagation [10], and gives rise to unique chiral and topological magnetic structures like magnetic spirals and skyrmions. Both ab initio calculations [11], focusing on ideal stacks, and experimental studies [12] support the view that iDMI represents an interface magnetic energy. The sign of iDMI holds of a significant importance since it determines the chirality of the interface. Additionally, maximizing PMA is crucial for reducing the size of spintronic devices used in data storage and for stabilizing domain walls and skyrmions with varying chirality when combined with iDMI. Magnetic damping is another essential material parameter that plays pivotal roles in numerous spintronic applications. These magnetic material parameters need to

be precisely defined and tuned based on the specific requirements of the intended application. Therefore, several HM/FM have undergone experimental testing. It is important to note that the FM film possesses two interfaces, making it challenging to disentangle the dual contributions to these three material parameters in a given 'bottom layer/FM/top layer' structure. Furthermore, the temperature exerts a significant influence on the magnetic properties of diverse materials, especially in the case of ultra-thin films. Temperature not only offers an effective avenue for exploring the interplay between these parameters but also serves as a valuable tool for comprehending their physical origins and assessing the performance of spintronic devices under elevated temperatures. Additionally, there is an anticipation that electronic devices might operate efficiently across a broader temperature range, extending beyond room temperature. Hence, the focus of this paper is to explore damping, perpendicular magnetic anisotropy, and interfacial Dzyaloshinskii-Moriya interaction in Cu/Fe- and Pt/Fe-based systems. Special attention is given to the impact of temperature as well as the underlayer and the capping layers. The objective is to employ various materials and different combinations or stacking orders to discern the distinct contributions to PMA, iDMI, and damping. To achieve this, ferromagnetic resonance (FMR), Brillouin light scattering (BLS) coupled with vibrating sample magnetometry (VSM) techniques were utilized.

II- Samples and experimental techniques

The studied samples are 5×5 mm^2 in lateral size and have the structure Si/SiO_2/Ta (2.5)/X/Fe(t_{Fe})/Y/Ta (2.5), where X=Pt (4), Ir (4) and Cu (2), Y=Ir (4), Cu (2) and MgO (1), $1.4\ \text{nm} \leq t_{Fe} \leq 10\ \text{nm}$, and the numbers in parentheses represent the thickness in nm. The samples were grown using a magnetron sputtering system with a base pressure lower that 2×10^{-8} Torr. The metallic layers were deposited using dc sputtering under an Ar pressure of 1.5 mTorr, while the 1 nm thick MgO layer was grown by rf sputtering in an Ar pressure of 10 mTorr. Hysteresis loops were measured under in-plane and perpendicular applied magnetic

fields using a vibrating sample magnetometer (VSM) for each sample with a given Fe thickness. The saturation magnetic moment per unit area ($M_s \times t_{Fe}$) is then determined and used to obtain the magnetization at saturation (M_s) and the thickness of the magnetic dead layer (t_d) for each system. To investigate iDMI and PMA versus temperature, BLS [13] in Damon-Eshbach configuration was employed to record spectra for a given field and spin wave vector (see supplementary). For this purpose, the temperature was varied from the room temperature (RT) to 250°C and the spectra under a magnetic field applied in the plane of the samples were recorded. Microstrip FMR (MS-FMR) [14] was used to investigate PMA and damping (see supplementary) at RT and post-temperature BLS measurements.

III- Results and discussions

1- Room temperature measurements

This section is devoted for the RT static and dynamic magnetic properties. We first use VSM to obtain magnetization at saturation and the thickness of the magnetic dead layer, crucial parameters for the precise determination of PMA and iDMI constants as well as spin pumping efficiency. These latter are then investigated and discussed to evidence the contribution of the two magnon scattering contribution to damping and separate the contribution of each interface with Fe to the total iDMI and interface PMA.

a- Static properties

Figure 1 shows the Fe thickness dependence of $M_s \times t_{Fe}$ for all the systems. The linear fits allow determining the magnetization at saturation and the thickness of the magnetic dead layer from the slope and the horizontal axis intercept, respectively. Table 1 summarizes the obtained values for M_s and t_d. One can note the absence of a magnetic dead layer for Pt/Fe/Cu and slightly low t_d values for Ir/Fe/MgO (t_d=0.2 nm), Ir/Fe/Cu (t_d=0.32 nm) and Cu/Fe/Cu (t_d=0.25 nm). The higher t_d values, of Pt/Fe/Ir (t_d=0.5 nm) and Cu/Fe/Ir (t_d=0.8 nm), allowed concluding that the thicker magnetic dead layers are associated with the presence of Ir

capping or buffer layer and with the Cu buffer layer. A simple analysis of t_d allows deducing a zero magnetic dead layer for Pt/Fe, a negligible oxidation or intermixing at Fe/MgO and Fe/Cu interfaces and a thicker magnetic dead layer at Fe/Ir and Cu/Fe interfaces compared to those of Ir/Fe and Fe/Cu, respectively. This suggests more interdiffusion at the Fe/Ir upper and Cu/Fe bottom interfaces. M_s values, shown in table 1, are slightly lower than that of bulk Fe (1700 emu/cm^3) [15]. M_s varies slightly with stacks: while similar values are obtained for Ir/Fe/Cu, Pt/Fe/Cu, Pt/Fe/Ir and Cu/Fe/Cu, a decrease of the M_s is revealed for Ir/Fe/MgO sample. This can most likely be attributed to the interpenetration of oxygen into Fe during the deposition of MgO [16].

The largest M_s value (M_s=1677 emu/cm^3) has been observed for Cu/Fe/Ir. It is worth mentioning that the slope of the thickness dependence of $M_s \times t_{Fe}$ for this system changes at a thickness of 2.4 nm (see the inset of figure 1), suggesting a change of M_s at a critical Fe thickness. Indeed, t_d= 1.35 nm and M_s=2650 emu/cm^3 when the thinner regime ($t_{Fe} \leq$ 2.4 nm) is used for fitting, whereas t_d= 0.85 nm and M_s=1677 emu/cm^3 for the thicker range. This change of M_s could be attributed to a decrease in Curie temperature or to a structural change during the growth. Indeed, structural differences, such as amorphous Fe for the thickest regime and (partially) textured polycrystalline Fe for the thinnest thickness regime may explain the change in M_s below and above a certain critical Fe thickness. Temperature dependence of $M_s \times t_{Fe}$ will be helpful to check whether the slope change also takes place at very low temperatures and therefore identify the origin of this slope change. Although we have no direct evidence of such a structural change for these films, we believe that such structural changes for these thin films may occur at the first atomic planes. For simplicity, all the measurements presented below for this system are analyzed by considering M_s=1677 emu/cm^3 and t_d=0.8 nm (parameters deduced from the fit of $M_s \times t_{Fe}$ of thick samples: above 2.4 nm) to deduce PMA, iDMI parameters and to investigate the thickness dependence of

damping. It is noteworthy to highlight the superior quality of samples achieved with the Pt underlayer layer, attributed to the presence of the Ta seed layer. The Ta seed layer contributes to an atomically smoother interface with Pt compared to Cu and Ir. Therefore, we can draw the conclusion that employing an appropriate buffer layer can enhance the interface quality by minimizing roughness and significantly influencing the magnetic properties.

b- PMA and damping

We will now first focus on the PMA and the Gilbert damping. For this aim, MS-FMR measurements were performed and analysed following the procedure presented in the supplementary. The effective magnetization (M_{eff} defined as $\mu_0 M_{eff} = \mu_0 M_s - \frac{2K_\perp}{M_s}$, where $K_\perp$ is the PMA constant) for all systems with the various capping and buffer layers is shown in figure 2 versus the inverse of the Fe effective thickness, defined as $t_{eff}=t_{Fe}-t_d$. One can observe a significant linear thickness dependence of $\mu_0 M_{eff}$ with a slope and a vertical intercept affected by the buffer and the capping layers. This suggests the existence of an interfacial contribution to the PMA. Note the deviation from the linear behavior for the thinner Fe films, most likely due to the interface quality degradation as the thickness is reduced, especially for Cu/Fe/Cu and Ir/Fe/Cu. The linear dependence of $\mu_0 M_{eff}$ versus $1/t_{eff}$ suggests that $K_\perp$ can be described by the phenomenological relationship $K_\perp = K_v + \frac{K_s}{t_{eff}}$, where K_s and K_v are the perpendicular uniaxial surface and volume anisotropy constants, respectively. K_v and K_s are straightforwardly obtained from the vertical intercept and from the slope of the linear fit of $\mu_0 M_{eff}$ versus $1/t_{eff}$, as summarized in table 1. At this stage, it is challenging task to precisely delineate the contribution of each interface with Fe to the total value of K_s presented in Table 1, unless we assume that the interfaces with Fe involving the same material as a capping or buffer layer are symmetrical. Thus, more information about K_s is required, and this specific contribution will be addressed later following the investigation of iDMI.

As explained in the supplementary material, the frequency dependences of the FMR field half linewidth at half maximum (ΔH) revealed a significantly different behavior for the samples with the thicker Fe layers (10 nm). It is characterized by a nonlinear variation while no obvious significant nonlinear contribution is observed for the thinner Fe films. This non-linearity is attributed to two magnon scattering (TMS) by the defects or dislocations [17-21] as confirmed by the lower slope of the frequency dependence of ΔH in perpendicular applied magnetic field (see figure S2-3c in supplementary). These perpendicular-field linewidth measurements were only possible for some few systems with thinner Fe films, due to the low signal-to-noise ratio in this configuration and the weak magnetic field available on our set up ‘see supplementary). Therefore, the lack of the nonlinearity in the frequency dependence of the in-plane ΔH of the thinner Fe films combined with the impossibility of measuring ΔH with a perpendicular applied magnetic field prevent fitting of the experimental data including all contributions ΔH. Therefore, for these samples showing a linear behavior of ΔH, the linear fit is used to deduce the effective value of damping (α_{eff}). The variations of the effective damping constant α_{eff} as a function of $1/t_{eff}$ are shown in figure 3a for all systems. Two different trends are observed: while almost a linear dependence of α_{eff} versus $1/t_{eff}$ is revealed for Ir/Fe/MgO, a nonlinear behavior is observed for Cu/Fe/Ir, Cu/Fe/Cu, Pt/Fe/Cu and Ir/Fe/Cu. Note the markedly nonlinearity in the systems with Cu buffer layer, indicating that TMS is the dominant relaxation mechanism for the thinnest films of the series. The highest damping values were obtained for Cu/Fe/Ir, suggesting a stronger TMS contribution, whereas Pt/Fe/Cu system shows the lowest values. Furthermore, note the thickness dependence of α_{eff} of Cu/Fe/Cu where a negligible amount of spin pumping is expected, confirming again that the TMS mechanism is behind this behavior. We thus consider that the total damping in all the studied systems can be understood as the sum of the “intrinsic” damping (α_{Fe}) of Fe layer and the interfacial damping, including spin pumping (characterized by a linear dependence

with $1/t_{eff}$) and two-magnon scattering processes, given by $\alpha=\alpha_{Fe}+\alpha_P+\alpha_{TM}$. The spin pumping induced-damping contribution is $\alpha_P = \frac{g\mu_B}{4\pi M_s t_{eff}} g_{eff}^{\uparrow\downarrow}$ (where μ_B is the Bohr magneton and $g_{eff}^{\uparrow\downarrow}$ is the effective spin mixing conductance) whereas $\alpha_{TM} = \frac{\beta_{TM}}{t_{eff}^2}$ is the interfacial TMS damping arising from the magnetic roughness. Indeed, this interfacial two magnon scattering, is expected to be proportional to $\frac{1}{t_{eff}^2}$ because the two magnon scattering scales with the square of the scattering potential, which is proportional to the inverse of the ferromagnetic film thickness [22].

The fits of the experimental data give α_{Fe}, β_{TM} (which parameterizes the strength of the TMS) and $g_{eff}^{\uparrow\downarrow}$ as summarized in table 1. For Pt/Fe/Ir and in the lack of more experimental data for thinner Fe layers (due to the weak MS-FMR signal due to the large damping values), it is difficult to evaluate β_{TM}. β_{TM} is strong in Cu/Fe/Cu and Cu/Fe/Ir systems and slightly lower for the other systems. It is known to be dependent on the surface conditions of ferromagnetic films, including the surface roughness and the surface magnetic anisotropy [23, 24]. The variations of β_{TM} as a function of $\left(\frac{2K_s}{M_s}\right)^2$ are shown in figure 3b where an accurate linear scaling is observed, in good agreement with the expectation for two magnon scattering $\beta_{TMS} = C_{TM}\left(\frac{2K_s}{M_s}\right)^2$ [25]. This indicates mostly a similar magnetic roughness of interfaces and correlation of β_{TM} with the interfacial magnetic anisotropy. This is good agreement with the higher ΔH in perpendicular applied magnetic field compared to the one measured in-plane, attributed to interface PMA inhomogeneity. The obtained values of C_{TM} (0.016 T^2) is very lower compared to that of HM/FM/oxides (0.08 T^2) [25] and the reported value (0.18 T^2) by Yoshii et al. [26]. Note the weak two magnons scattering of Ir/Fe/MgO despite the strong of both the spin-orbit coupling and the interfacial PMA in agreement with the observed behavior in Ta/Co/MgO [25]. It is worth mentioning the correlation between the thin magnetic dead

layer and strength of TMS: this latter is weak or even negligible for Pt/Fe/Cu and Ir/Fe/MgO where t_d shows the lower values.

The obtained values of thickness independent damping of Fe (α_{Fe}) for all the samples is around 2×10^{-3}. This value is in good agreement with the reported one by Schoen el al. [27]. The higher α_{Fe} values of Cu/Fe/Ir and Cu/Fe/Cu are most probably effective damping value due to the strong two magnon scattering in these systems which leads to an overestimation of the intrinsic damping. Moreover, table 1 reveals that $g_{eff}^{\uparrow\downarrow}$, a key parameters governing the spin-dependent transport through the HM/FM interface, of Ir/Fe/Cu and Cu/Fe/Ir are slightly different. This confirms again the asymmetry of Fe/Ir and Ir/Fe interface: spin pumping efficiency is higher at Fe/Ir interface. Because spin pumping at Cu/Fe and Fe/MgO interfaces are negligible, we conclude on the significantly higher $g_{eff}^{\uparrow\downarrow}$ of Ir/Fe compared to Pt/Fe interface. The higher $g_{eff}^{\uparrow\downarrow}$ for Pt/Fe/Ir ($g_{eff}^{\uparrow\downarrow}$ =49.37±3 nm^{-2}) is in good agreement with the obtained values of Pt/Fe/Cu ($g_{eff}^{\uparrow\downarrow}$ =19.18± nm^{-2}) and Cu/Fe/Ir ($g_{eff}^{\uparrow\downarrow}$ =35.14±3 nm^{-2}).

c- Spin waves non reciprocity and PMA

iDMI constant in the systems including Pt and/or Ir has been determined by from the BLS measurements as explained in the supplementary material. The linear fit of the variation of D_{eff} versus $1/t_{eff}$ for the studied systems, shown in figure 4a, allowed determining D_s for each system, as shown in table 1. The analysis of obtained values revealed that the iDMI constants of the Fe/Cu and Cu/Fe interfaces are negligible. Moreover, Pt/Fe and Ir/Fe interfaces have an opposite iDMI sign: it is positive for Ir/Fe and negative for Pt/Fe. Taking into account the D_s values of the different systems shown in the table 1, we deduce $D_s^{Ir/Fe}$=0.27 pJ/m, $D_s^{Pt/Fe}$=-0.99 pJ/m and $D_s^{Fe/MgO}$=-0.17 pJ/m. This latter value is in good agreement with the deduced value by Zhang et al. ($D_s^{Fe/MgO}$=-0.15 pJ/m) [29] and those of Co/MgO ($D_s^{Co/MgO}$=-0.22 pJ/m) [30] and CoFeB/MgO ($D_s^{CoFeB/MgO}$=-0.17 pJ/m) [30] reported in [29, 30]. The obtained value of $D_s^{Ir/Fe}$ is also in good agreement with that of Co/Ir

($D_s^{Co/Ir}$=0.32 pJ/m) [31] but slightly lower than the reported value by Zhang et al. [32] (D_s ~ 0.6 pJ/m) for iDMI measurements at room temperature on Ir/Fe(3nm)/SiO_2. We should mention that iDMI is sensitive to disorder, defects and atom arrangement at the interfaces which vary significantly as a function of sample elaboration parameters, like deposition technique, underlayer and capping layer. Therefore, it is not surprising to have dispersion between experiments for the obtained values of iDMI since the sample elaboration and interface properties may differ.

It is worth noting the deviation from the linear behavior of D_{eff} versus $1/t_{eff}$ for the thicker Fe films (above 2.8 nm), suggesting other contributions to ΔF. Furthermore, for the 10 nm thick Fe layer, ΔF is negative for all the systems despite the different sign of their total iDMI. Therefore, this nonlinearity cannot be due to iDMI. Indeed, asymmetry of the magnetic film properties due to an interface PMA is known to induce spin wave non-reciprocity [33]. Therefore, iDMI always combines with the effect of the interface PMA difference because both contributions to the spin wave frequency obey the same symmetry [33]. According to Gladii et al. [33], the frequency non-reciprocity due to the interface PMA difference scales linearly with the wave vector and quadratically with the FM thickness for thicknesses of 20 nm and below. Since iDMI scales linearly with the inverse of FM thickness, ΔF of the thicker Fe layers (t_{Fe} > 2.8nm) results mostly from the difference in interface PMA between the lower and upper interfaces while it is induced by iDMI for the thinner Fe films. To separate the two contributions, we first consider ΔF of the thinner samples (t_{Fe} <2.8 nm) for each sample to determine D_{eff} and then D_s as indicated in table 1, since iDMI scales linearly with the inverse of Fe thickness. The variations of ΔF over the whole range of t_{Fe} were then fitted using $\Delta F = D_s \frac{4\gamma}{2\pi M_s t_{eff}} k_{sw} + \frac{8\gamma}{\pi^3} \frac{K_s^{bot} - K_s^{top}}{M_s} \frac{1}{1+\frac{\Delta^2\pi^2}{t_{eff}^2}} k_{sw}$, where $\Delta = \sqrt{\frac{2A_{ex}}{\mu_0 M_s}}$ is the exchange length and $\Delta K_s = K_s^{top} - K_s^{bot}$ is the difference in surface anisotropies of the top and the bottom interfaces with

Fe (see figure 5b), using ΔK_s as a fit parameters. This allowed deducing ΔK_s of the two interfaces with Fe as presented in table 1. Note the positive sign of ΔK_s and thus the higher surface anisotropy induced by the top interface with Fe for all the systems.

To separate the contribution of each interface with Fe to the perpendicular magnetic anisotropy, we combined the interface PMA constants difference between the top and bottom interfaces ($\Delta K_s = K_s^{top} - K_s^{bot}$) with the effective interface PMA constant ($K_s = K_s^{top} + K_s^{bot}$), values indicated in table 1. The obtained values for each interface are shown in table 2. The deduced values for Cu/Fe and Fe/Cu allowed evaluating the effective interface anisotropy constant of Cu/Fe/Cu ($K_s = K_s^{Cu/Fe} + K_s^{Fe/Cu}$=0.65+0.57 =1.22 mJ/m^2), which is in good agreement with the directly obtained value from the fit the thickness dependence of M_{eff} of this system given in table 1. Note the significant and the slight asymmetry of the Fe/Ir and Ir/Fe and Fe/Cu and Cu/Fe interfaces, respectively. The stronger interface anisotropies are induced by Fe/MgO and Fe/Ir while the weak interface anisotropy is obtained for Pt/Fe.

2- Temperature dependence measurements

In this section, we will focus on the effect of measurement temperature on PMA, iDMI and damping of Cu/Fe/Cu and Pt/Fe/Cu systems. Pt/Fe/Cu is chosen due to the strong iDMI induced by the single Pt/Ir while Cu/Fe/Cu is used as a symmetrical system showing both strong TMS and interface PMA. It is worth mentioning that our VSM setup does not allow temperature dependence measurements and therefore, for each temperature, we will consider M_s values at room temperature (RT) for the analysis of data as a function of temperature. The hypothesis of a constant M_s value that is independent of the temperature of measurements can be justified by the high Curie temperature of Fe (1044° K) [34] and the low measurement temperatures of this study (≤ 250°C). Indeed, for such temperature range, M_s change is less than 6%. Furthermore, in the absence of VSM measurements for each temperature, t_d values

of the as grown sample are considered for all temperatures to evaluate the effective Fe thickness used in the analysis of the experimental data.

The temperature dependences of K_s and D_s constants for Pt/Fe/Cu are shown in figures 5a and 5b. While K_s varies linearly over the entire temperature range up to 250°C, D_s shows a strong nonlinear dependence with the temperature. Moreover, in contrast to K_s, which increases by 20%, D_s decreases significantly, in absolute value, by approximately 60%, suggesting a greater sensitivity of iDMI to temperature. Similar trend where iDMI varies more strongly with temperature than PMA and M_s has been reported by Schlotter et al. [35] indicating that interfacial DMI is more sensitive to thermal fluctuations than bulk magnetic properties. This variation with temperature cannot be due to the weak M_s change in the range of RT-250°C. As mentioned above, interface anisotropy results mainly from the Fe/Cu interface, whereas iDMI is induced by the Pt/Fe interface. This could explain the difference in behavior between K_s and D_s suggesting that the Pt/Fe interface is more affected by the temperature during the measurement. In addition, at high temperatures, oxidation can also take place because samples are heated in air, leading to a reduction in M_s and may be responsible for the anisotropy increase.

We have also been interested in the correlation between iDMI and surface PMA. Ideally, this correlation could be investigated by studying the variation of K_s as a function of D_s as shown in figure 5c. It is worth mentioning that a linear fit of the data can be obtained, but the fit with a second-order polynomial reproduces the experimental data better. This could be due to the greater sensitivity of iDMI to interface anisotropy. Furthermore, as mentioned above, iDMI results mainly from the Pt/Fe interface, whereas K_s is induced by the Pt/Fe interfaces and predominantly by Fe/Cu which seems be less affected by temperature, hence the low variation. It is worth to mention that both K_s and D_s calculations involve a linear expression of M_s. Therefore, their correlation is less affected by M_s, which thus overcomes the need to

measure M_s as a function of temperature. Similar behaviors have been observed for the temperature dependence of both K_s and K_v of Cu/Fe/Cu systems (see figure 6) with a slightly weaker slope of K_s (1×10^{-3} mJ/m^2°C) compared to that of Pt/Fe/Cu (1.4×10^{-3} mJ/m^2°C). The temperature dependence of mean Stokes and anti-Skoes line widths, measured at a magnetic field of 0.2 T (see figure S4-2a in the supplement) revealed an irreversible increase, suggesting a structural evolution during heating, resulting from interdiffusion. The latter occurs mainly at the bottom interface, confirming the weak variation of K_s of Pt/Fe/Cu with temperature.

Several possible sources may be responsible for the physical origin of the observed behavior of the anisotropy and iDMI constants. In addition to the evolution of crystal structure during the measurements, atomic diffusion and lattice strain at interfaces could play a role in this behavior in the same way that thermal expansion of the lattice is a primary source of the temperature dependence of the Heisenberg exchange [36]. Moreover, using the extended droplet model, Kim et al [37] find that the DMI increases with decreasing temperature in a range from 300 to 100 K. Since the electron-phonon interaction promotes, in general, thermally-induced hopping between nearest neighbours when increasing the temperature, they expected that the difference between in-plane and out-of-plane hopping energies is reduced upon temperature increase. Therefore, changing the temperature of the system allows for charge redistribution between in-plane and out-of-plane orbitals, while preserving the major electronic state of the trilayer, which may cause a permanent atomic rearrangement and thus induce undesired extrinsic effects. Furthermore, the electron-phonon interactions and magnetization fluctuations lead to a broadening of the Fermi energy, affecting thus the temperature behavior of iDMI [37]. Finally, this temperature dependence, in particular that of D_s, could be due to the hybridization of orbitals 3d and 5d orbitals near the Fermi level and thermal disorder. As it will be discussed below and in the supplement material, the crystal

structural evolution of Pt/Fe/Cu during temperature cannot induce such large variation of D_s and we can conclude that electron-phonon interactions are the main source or the temperature dependence of D_s. The temperature dependence of M_s will be helpful to obtain the scaling of D_s with M_s and therefore, to more investigate the origin of the thermal dependence of iDMI constant.

To check the irreversible changes in the structural and magnetic properties of the samples, MS-FMR was used to determine the PMA constants and the magnetic damping coefficient after the temperature measurements had been completed. The obtained values were then compared with those deduced from MS-FMR measurements on the same samples before proceeding to temperature-dependent measurements. Figures 7a and 7b show the thickness dependences of the magnetic moment per unit area of as grown samples Pt/Fe/Cu and Cu/Fe/Cu (before heating) compared to those that have undergone a complete temperature measurement cycle (after heating). 0.22 nm and 0.52 nm thick magnetic dead layers appear after a complete heating cycle for Pt- and Cu-buffered samples, respectively. This suggests an interdiffusion that occurs at the Fe interfaces during the temperature measurement process. Indeed, as the temperature rises, interdiffusion is triggered and becomes more pronounced as the measurement time increases. This results in an intermixing of the interface atoms at and, consequently, the formation of a magnetic dead layer. Determining the precise factors governing the mixing between atoms at interfaces can be challenging. However, it appears that the atomic radius and electronegativity of the atoms play crucial roles in facilitating this phenomenon. Note the slope change at t_{Fe}=2.4 nm for Cu/Fe/Cu after heating in similar manner to the above-discussed trend. This suggests that this change of M_s at a critical thickness of Fe is most probably due to the structural enhancement of these thin films resulting from the prolonged exposure to increased temperature. This is in

good agreement with the slight increase in M_s after heating (M_s=1618 emu/cm^3 and M_s=1583 emu/cm^3 for Cu/Fe/Cu and Pt/Fe/Cu, respectively).

The linear fitting of the thickness dependences of the M_{eff} and iDMI constant as well as the damping fitting with the above-mentioned model taking into account the TMS contribution were used to obtain K_s, K_v, $g_{eff}^{\uparrow\downarrow}$, β_{TM} and D_s for both systems (see figures 7c and 7d). The obtained values of PMA constants (from the MS-FMR measurements) for Pt/Fe/Cu, before (K_s=0.82 mJ/m^2 and K_v=0.22×10^5 J/m^3) and after a complete heating process (K_s=0.81 mJ/m^2 and K_v=0.69×10^5 J/m^3), show that only the volume anisotropy changed. Furthermore, the obtained values for the Fe damping, β_{TM} and iDMI constant after heating are found to be α_{Fe}=4.8×10^{-3}, β_{TM}=1.6×10^{-2} nm^2, $g_{eff}^{\uparrow\downarrow}$=19.1 nm^{-2} and D_s=-0.8 pJ/m (see figure S4-2b in the supplement). α_{Fe} is considerably higher than that obtained before heating, most probably due to the atomic interdiffusion. In contrast to the other interface parameters (K_s and $g_{eff}^{\uparrow\downarrow}$), D_s and β_{TM} have decreased slightly after heating, again suggesting the stronger temperature dependence of iDMI compared to K_s and $g_{eff}^{\uparrow\downarrow}$. These temperature-dependent measurements result in a significant change in the bulk magnetic properties, such as the volume anisotropy and damping constants, after heating while interface properties are less affected. In the case of Cu/Fe/Cu, the obtained values for K_s and K_v are shown in figure 6 in blue triangles indicating a slight increase compared to those measured prior to heating, suggesting an improvement in the structural quality of the samples with heating. Moreover, besides the increase of Fe damping, a significant increase of β_{TM} (β_{TM} =5.6×10^{-2} nm^2) is obtained after heating, probably due to the interdiffusion that occurs at interfaces with Cu.

Conclusion

We experimentally investigated the interfacial magnetic properties of Fe-based systems with various capping and buffer layers. Our findings indicate that it is possible to deduce the individual interface contributions to the perpendicular magnetic anisotropy. This can be

achieved by combining the effective interface constants and differences in interface anisotropy between the top and bottom interfaces with Fe, obtained from the thickness dependences of the effective magnetization and spin waves frequency mismatch of the thicker Fe films, respectively. The FMR linewidth measurements under an in-plane applied magnetic field suggested the presence of an additional extrinsic damping caused by the interfacial two-magnon scattering. This was correlated with interface magnetic anisotropy. Furthermore, the thickness dependence of the effective interfacial Dzyaloshinskii-Moriya interaction (iDMI) constant was investigated, allowing for the separation of contributions from the various interfaces. Our results show that Ir/Fe and Fe/MgO interfaces induce weak iDMI of opposite signs, contributing to the total iDMI. The temperature dependence of iDMI, damping and interface PMA in Pt/Fe/Cu and Cu/Fe/Cu thin films, which is of crucial importance for the potential spintronic applications were carried out. It revealed an increase of both damping and PMA constant with temperature and a significant decrease of iDMI due to the increased thermal fluctuations. This suggests that iDMI is more strongly sensitive to temperature, prompting further questions about the specific sources of the temperature dependence of iDMI and the impact of structural changes on its behavior.

Acknowledgements

We acknowledge the French National Research Agency for financial support within the ANR program EHIS (ANR-21-CE42-0003). M S G acknowledges the financial support for this work from MRID, CNCS/CCCDI—UEFISCDI, through Grant PN-III-P4-ID-PCE-2020-1853-SPINSYNE.

References

[1] A. Soumyanarayanan, N. Reyren, A. Fert and C. Panagopoulos, Nature 539, 509 (2016).

[2] P. M. Haney and M. D. Stiles, Phys. Rev. Lett. 105, 126602 (2010)

[3] M.T. Johnson, R. Jungblut, P.J. Kelly, F.J.A. den Breeder, J Magn. Magn. Mat. 148, 118 (1995).

[4] B. Dieny and M. Chshiev, Rev. Mod. Phys. 89, 025008 (2017).

[5] R.H. Zhao, Z.Y. Ren, J.P. Cao, Y.S. Yuan, G.L. Zhao, X.G. Xu, K.K. Meng, J. Miao, Y. Jiang, Solid State Comm. 332, 114340 (2021).

[6] Y. Tserkovnyak, A. Brataas, G. E. Bauer, Phys. Rev. Lett. 88, 117601 (2002).

[7] M. Shen, X. Li, Y. Zhang, X. Yang and S. Chen, J. Phys. D: Appl. Phys. 55 213002 (2022).

[8] J. Sinova, S. O. Valenzuela, J. Wunderlich, C. H. Back, and T. Jungwirth, Rev. Mod. Phys. 87, 1213 (2015).

[9] D. Mancilla-Almonacid, R. Jaeschke-Ubiergo, A. S Núñez and S. Allende, Nanotechnology 31, 125707 (2020)

[10] F. Ma a and Y. Zhou, Royal Soc. Chem. Adv. 4, 46454 (2014).

[11] H. Yang, A. Thiaville, S. Rohart, A. Fert and M. Chshiev Phys. Rev. Lett. 115, 267210 (2015).

[12] J. Cho, N-H. Kim, S. Lee, J-S. Kim , R. Lavrijsen , A. Solignac, Y. Yin, D-S. Han , N. J. J. van Hoof, H. J.M. Swagten, Be. Koopmans and C-Y. You, N. Comm. 6, 7635 (2015).

[13] M. Belmeguenai, M. S. Gabor, Y. Roussigné, A. Stashkevich, S. M. Chérif, F. Zighem, and C. Tiusan, Phys. Rev. B 93, 174407 (2016).

[14] M Belmeguenai , M S Gabor , F Zighem , N Challab, T Petrisor Jr, R B Mos and C Tiusan, J. Phys. D: Appl. Phys. 51 045002 (2018).

[15] J.-M. L. Beaujour, A. D. Kent, D. W. Abraham, and J. Z. Sun, J. Appl. Phys. 103, 07B519 (2008)

[16] H. K. Gweon, S. J. Yun and S. H. Lim, Sci. Rep. 8, 1266 (2018).

[17] R. D. McMichael, D. J. Twisselmann, and A. Kunz, Phys. Rev. Lett. 90, 227601 (2003).

[18] M. J. Hurben and C. E. Patton, ‘Theory of two magnon scattering microwave relaxation and ferromagnetic resonance linewidth in magnetic thin films’, J. Appl. Phys., 83, 4344 (1998).

[19] J. Lindner, K. Lenz, E. Kosubek, K. Baberschke, D. Spoddig, R. Meckenstock, J. Pelzl, Z. Frait, and D. L. Mills ‘Non-Gilbert-type damping of the magnetic relaxation in ultrathin ferromagnets: Importance of magnon-magnon scattering’, Phys. Rev. B 68, 060102(R) (2003).

[20] S. Wu, D. A. Smith, P. Nakarmi, A. Rai, M. Clavel, M. K. Hudait, J. Zhao, F. M. Michel, C. Mewes, T. Mewes, and S. Emori, Phys. Rev. B 105, 174408 (2022).

[21] J. Lindner, I. Barsukov, C. Raeder, C. Hassel, O. Posth, R. Meckenstock, P. Landeros, and D. L. Mills, ‘Two-magnon damping in thin films in case of canted magnetization: Theory versus experiment’, Phys. Rev. B 80, 224421 (2009).

[22] J. B. Mohammadi, J. M. Jones, S. Paul, B. Khodadadi, C. K. A. Mewes, T. Mewes and C. Kaiser, Phys. Rev. B 95, 064414 (2017).

[23] R. Arias and D. L. Mills, Phys. Rev. B 60, 7395 (1999).

[24] A. Azevedo, A. B. Oliveira, F. M. de Aguiar, and S. M. Rezende, Phys. Rev. B 62, 5331 (2000).

[25] L. Zhu, L. Zhu, D.C. Ralph and R.A. Buhrman, Phys. Rev. Appl. 13, 034038 (2020).

[26] S. Yoshii, Ke. Kato, E. Shigematsu, R. Ohshima, Y. Ando, K. Usami and M. Shiraishi, Phys. Rev. B, 106, 174414 (2022).

[27] M. A. W. Schoen, D. Thonig, M. L. Schneider, T. J. Silva, H. T. Nembach, O. Eriksson, O. Karis and J. M. Shaw, NATURE Phys. 12, 839 (2016)

[28] D. Ourdani, Y. Roussigné, S. M. Chérif, M. S. Gabor, and M. Belmeguenai, J. Phys. D: Appl. Phys. 55, 485004 (2022)

[29] W. Zhang, B. Jiang, L. Wang, Y. Fan, Y. Zhang, S.Y. Yu, G.B. Han, G.L. Liu, C. Feng, G.H. Yu, S.S. Yan, and S. Kang, Phys. Rev. App. 12, 064031 (2019).

[30] X. Ma, G. Yu, C. Tang, X. Li, C. He, J. Shi, Kang L. Wang, and Xiaoqin Li, Phys. Rev. Lett. 120, 157204 (2017).

[31] I. Benguettat-El Mokhtari, D. Ourdani, Y. Roussigné, R. B. Mos, .M Nasui, F. Kail, L Chahed, S. M. Chérif, A. Stashkevich, M. Gabor, and M. Belmeguenai, J. Phys.: Condens. Matter 32, 495802 (2020).

[32] W. Zhang, B. Jiang, L. Wang, Y. Fan, Y. Zhang, S.Y. Yu, G.B. Han, G. L. Liu, C. Feng, G. H. Yu, S.S. Yan and S. Kang, Phys. Rev. Appl. 12, 064031 (2019).

[33] O. Gladii, M. Haidar, Y. Henry, M. Kostylev, M. Bailleul, Phys. Rev. B, 93, 054430 (2016).

[34] J. Crangle and G. M. Goodman, Proc. Roy. Soc. Lond. A. 321, 477-491 (1971).

[35] S. Schlotter, P. Agrawal, and G. S. D. Beach, 'Annealing effect of sputter-grown Pt/$Ni_{80}Fe_{20}$/Pt sandwich trilayer films on Gilbert damping', J. Appl. Phys. 128, 223901 (2020).

[36] T. Brawell, J Phys. : Cond. Matt. 2, 7527 (1990).

[37] S. Kim, K. Ueda, G. Go, P-H. Jang, K-J. Lee, A. Belabes, A. Manchon, M. Suzuki, Y. Kotani, T. Nakamura, K. Nakamur, T. Koyama, D. Chiba, K. T. Yamada, D-H. Kim, T. Moriyama, K-J. Kim and T. Ono, Nature communications 9, 1648 (2018).

System	M_s(emu/cm^3)	t_d(nm)	K_v (x10^{5}J/m^3)	K_s (mJ/m^2)	α_0(x10^{-3})	$g_{eff}^{\uparrow\downarrow}(nm^{-2})$	β_{TM} (nm^2)	D_s (pJ/m)	ΔK_s(mJ/m^2)
Ir/Fe/MgO	1484	0.2	-0.93±0.007	1.28±0.02	2.1±0.4	31.95±2	n.d	0.096±0.003	0.36±0.03
Ir/Fe/Cu	1568	0.32	-0.12±0.001	1.02±0.02	2±0.2	29.88±2	0.024±0.003	0.27±0.006	0.2±0.02
Pt/Fe/Cu	1590	0	0.22±0.002	0.87±0.03	2±0.3	19.18±2	0.02±0.003	-0.99±0.04	0.2±0.02
Pt/Fe/Ir	1540	0.5	-0.39±0.002	1.09±0.02	1.8±0.2	49.37958±3	n.d	-1.28±0.05	0.5±0.03
Cu/Fe/Ir	1677	0.8	2.43±0.02	1.49±0.03	4±0.4	35.14±3	0.055±0.005	-0.25±0.006	0.2±0.02
Cu/Fe/Cu	1566	0.25	1.59±0.03	1.33±0.07	5±0.5	0	0.043±0.005		

Table 1: Parameters obtained from the best fits of the effective magnetization, the effective damping and the effective iDMI constant versus the inverse of the effective thickness of Fe thin films grown on Si substrates using various buffer and capping layers. n.d is used for not determined.

$K_S^{Fe/Cu}$(mJ/m^2)	$K_S^{Cu/Fe}$(mJ/m^2)	$K_S^{Pt/Fe}$(mJ/m^2)	$K_S^{Fe/Ir}$(mJ/m^2)	$K_S^{Fe/MgO}$(mJ/m^2)	$K_S^{Ir/Fe}$(mJ/m^2)
0.57 ± 0.04	0.65 ± 0.05	0.29 ± 0.04	0.8 ± 0.05	0.82 ± 0.05	0.43 ± 0.03

Table 2: interface anisotropy constants for the different interfaces with Fe obtained from the combination of ΔK_s and K_s values indicated in table1.

Fig. 1: Ourdani et al.

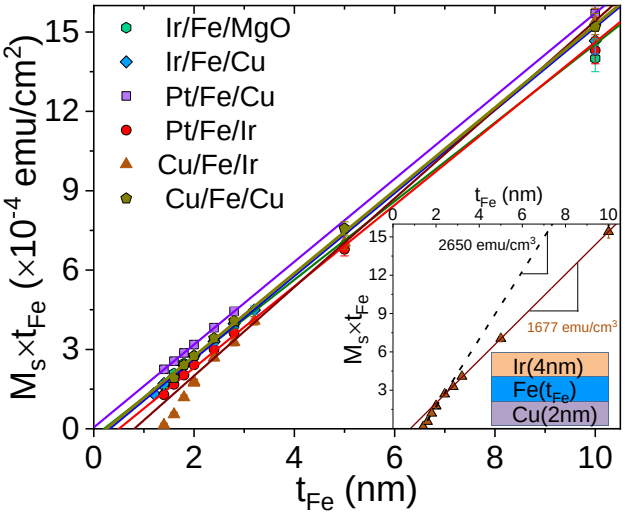

Fig. 2: Ourdani et al.

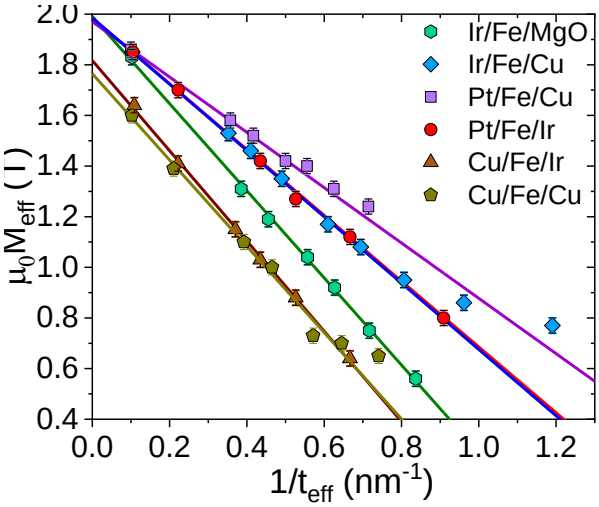

Fig. 3: Ourdani et al.

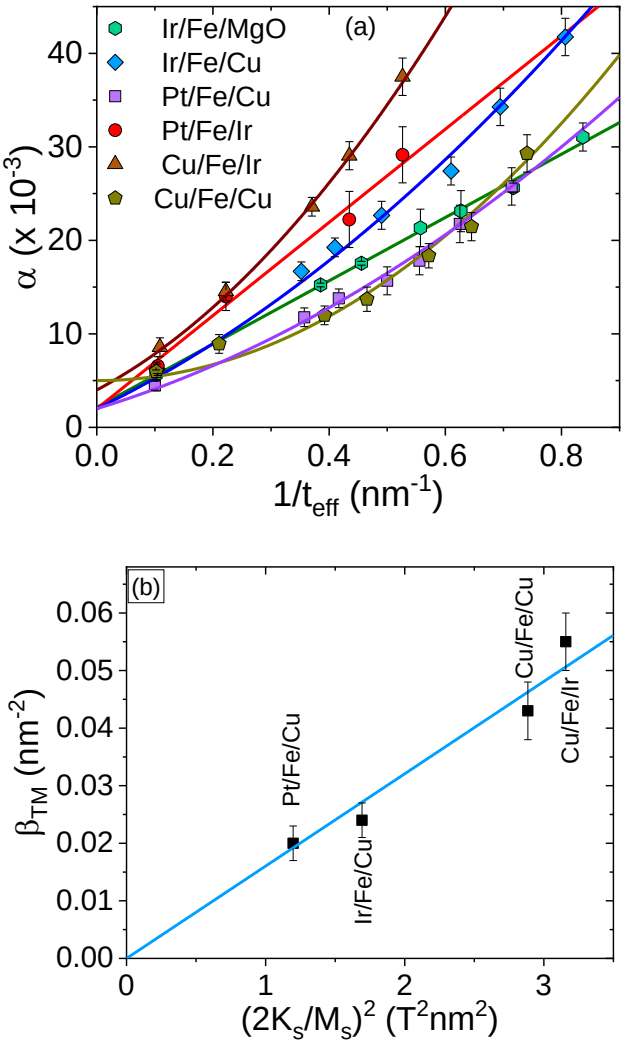

Fig. 4: Ourdani et al.

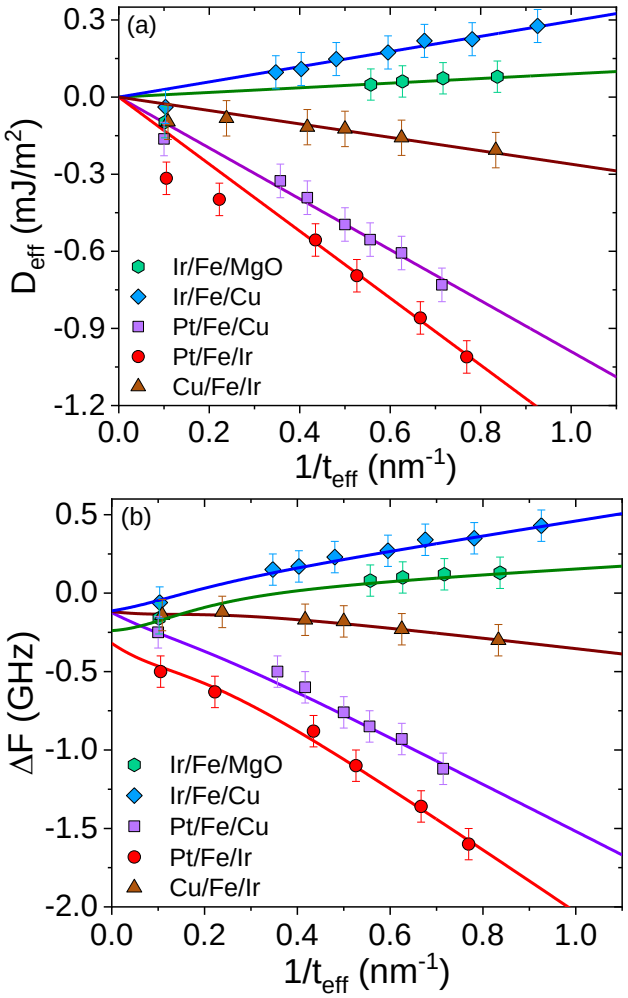

Fig. 5: Ourdani et al.

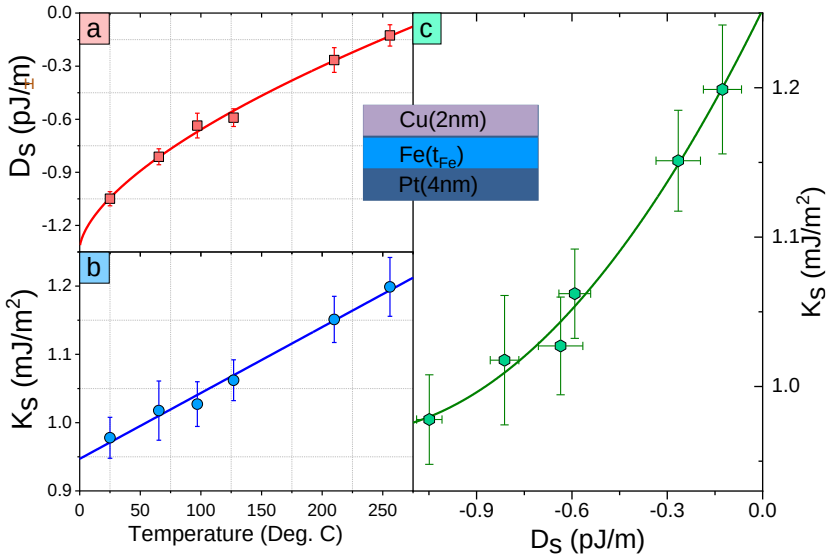

Fig. 6: Ourdani et al.

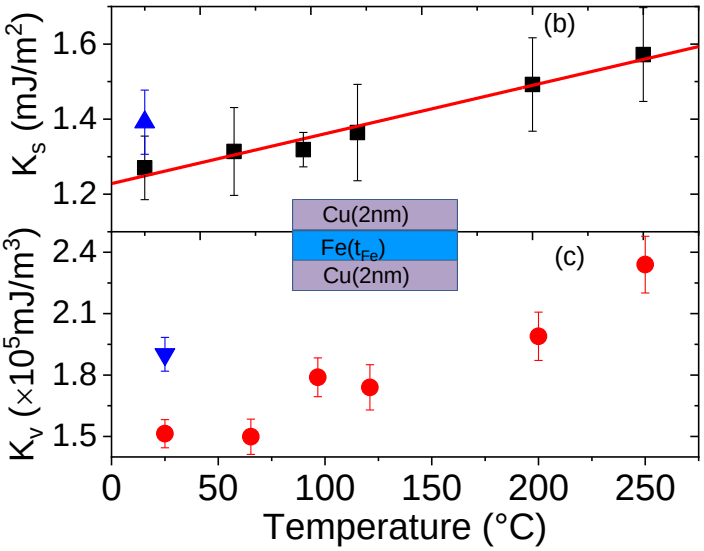

Fig. 7: Ourdani et al.

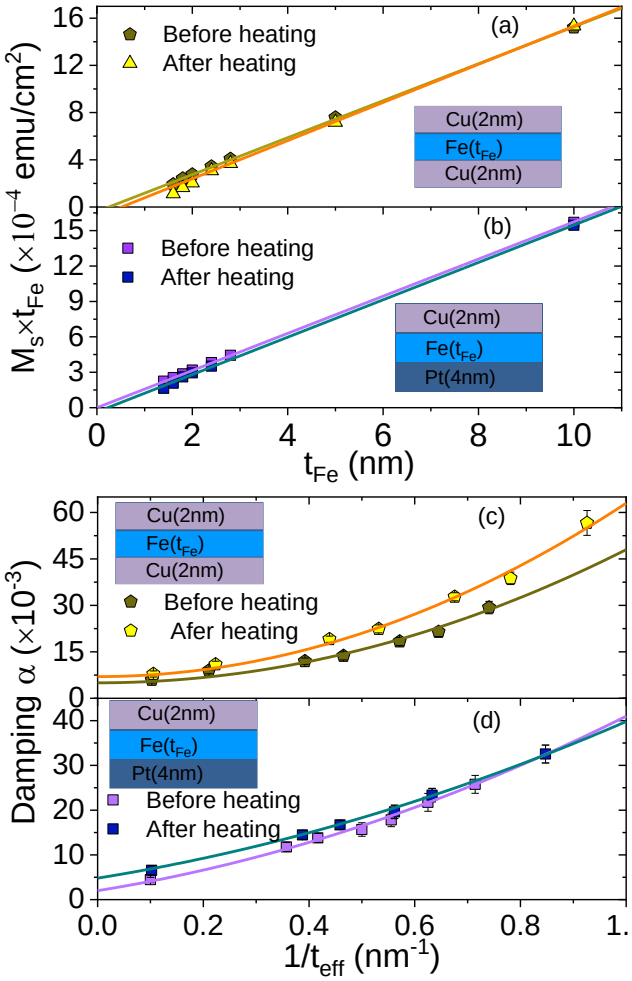

Figure captions

Figure 1:

Variation of the saturation magnetic moment per unit area versus the Fe thickness (t_{Fe}) for Fe-based systems with various buffer and capping layers grown on Si substrates. Symbols are VSM measurements and lines refer to the linear fits. The inset shows the corresponding data for Cu/Fe/Ir to illustrate the change of the slop of the linear dependence.

Figure 2:

Effective magnetization ($4\pi M_{eff}$) versus the Fe inverse effective thickness ($1/(t_{Fe}-t_d)$) for Fe-based systems with various buffer and capping layers grown on Si substrates. $4\pi M_{eff}$ values have been extracted from the fit of FMR measurements of the frequency of the uniform precession mode versus the in-plane applied magnetic field. Symbols refer to experimental data while solid lines are the linear fits taking into account only the thicker films.

Figure 3:

(a) Effective magnetic damping parameter deduced from the in-plane applied magnetic field measurements, as a function of the inverse of the Fe effective thickness of the different studied systems. Symbols refer to the experimental data and solid lines are linear fits or fits using the model described in the paper text. (c) Variation of the two magnon scattering

strength β_{TMS}versus $\left(\frac{2K_s}{M_s}\right)^2$. Symbols refer to data deduced from fits of figure (a) and solid lines are linear fits.

Figure 4:

Variation of (a) the effective iDMI constants and (b) the frequency shift between the Stokes and anti-Stokes lines (ΔF), measured at $k$sw=20.45 μm^{-1} as a function of the Fe inverse effective thickness of Fe-based systems with various buffer and capping layers grown on Si substrates. Solid lines refer to the linear fits and symbols are experimental data. Symbols are experimental data while solid lines refer to fits using equations given in the paper text.

Figure 5:

Temperature dependence of (a) the surface iDMI and (b) the interface PMA constants of the Pt/Fe/Cu samples grown on Si substrates. (c) Corresponding variation of the interface PMA versus the surface iDMI constants traducing their ccorrelation. Solid lines refer to fits (linear or nonlinear) and symbols are experimental data.

Figure 6:

Variations of perpendicular interface and volume anisotropy constants of the Cu/Fe/Cu system as a function of temperature. The blue triangles represent values obtained after a complete temperature measurements cycle.

Figure 7:

Variation of the saturation magnetic moment per unit area versus the Fe thickness for (a) Cu/Fe/Cu and (b) Pt/Fe/Cu samples before and after a complete temperature measurement cycle (room-temperature-250°C). Symbols are VSM measurements and lines refer to the linear fits. Effective magnetic damping parameter as a function of the inverse of for (c) Cu/Fe/Cu and (d) Pt/Fe/Cu samples before and after a complete temperature measurement cycle. Symbols refer to the experimental data and solid lines are fits using the model described in the paper text.